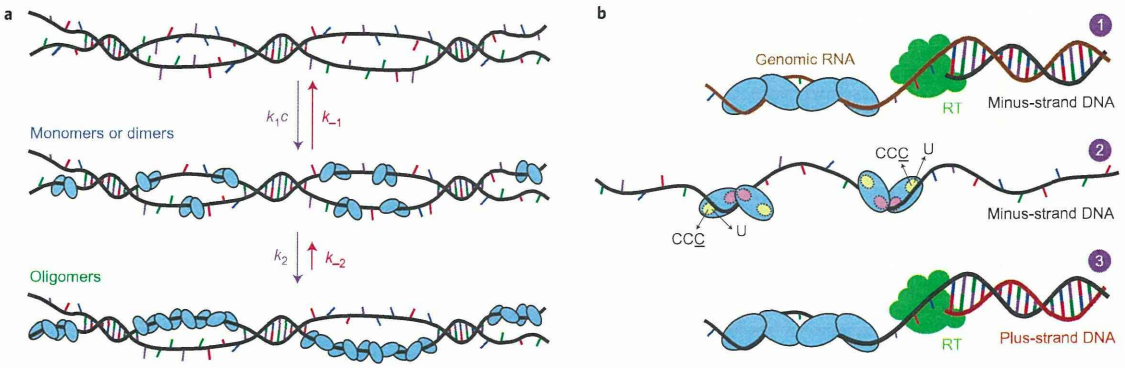

Figure 5 | Models for A3G oligomerization *in vitro* and *in virio*. a, *In vitro*, initially, monomers or dimers bind ssDNA with on rate k_1c and off rate k_{-1}. These forward and backward rates are on similar timescales ($1/k_1c = 33 \pm 1$ s at 200 nM A3G, and $1/k_{-1} = 85 \pm 5$ s), so fast binding reaches equilibrium before the monomers or dimers convert to oligomers ($1/k_2 = 149 \pm 13$ s) on ssDNA. Oligomer dissociation is significantly slower ($1/k_{-2} = 10 \pm 2$ h) *in vitro*. **b**, *In virio*, A3G oligomerizes on the RNA genome, blocking minus-strand DNA synthesis by RT (drawing 1). Once the oligomer dissociates, the monomers or dimers released bind ssDNA within a second, allowing rapid enzymatic activity (drawing 2) until A3G oligomerizes on the ssDNA template in 150 s and blocks plus-strand synthesis (drawing 3).

demonstrate that an A3G mutant (F126A/W127A) that is severely compromised in oligomerization, but retains deaminase activity, does not exhibit slow binding kinetics. Furthermore, a recent study shows that a similar oligomerization-defective mutant (W127A) inhibits deamination-independent viral restriction[44]. These observations support the hypothesis that A3G oligomerization is responsible for deaminase-independent inhibition of viral replication.

In light of these quantitative results *in vitro*, we propose a model for the effects of A3G on HIV-1 replication. A3G oligomerizes on viral RNA when it is packaged inside the virion[43,45], stalling RT during minus-strand synthesis. RT pauses until the oligomer dissociates, or switches to the other RNA template strand, circumventing the A3G roadblock and leading to partial inhibition of reverse transcription[35]. In contrast to our *in vitro* studies, the maximum size of the A3G oligomer may be limited by the small number of A3G molecules packaged in virions[36]. These limitations on oligomer size may lead to higher off rates *in virio*. Once the A3G oligomer dissociates during minus-strand synthesis, the monomers or dimers that are released have low affinity for the newly formed RNA–DNA duplex[14,19]. As RNase H activity exposes the minus-strand, all A3G molecules bind the ssDNA template within a second, as indicated by $1/k_1 = 0.7 \pm 0.1$ s when fast binding rates are extrapolated to the estimated 13 ± 8 μM A3G concentration in the virion[32]. A3G remains bound in a rapid sliding mode[37,41] for $1/k_{-1} = 85 \pm 5$ s, which allows high deamination rates[37,38] until oligomerization forms a roadblock to plus-strand synthesis after $1/k_2 = 149 \pm 13$ s (Fig. 5b).

The *in virio* model that we propose based on our measurements is consistent with the available data on A3G function. Recent cell-based experiments demonstrate that A3G uniformly blocks minus-strand synthesis in the absence of preferred RT termination sites along the viral template[35]. However, this does not necessarily indicate that A3G binds throughout the length of the genomic RNA. Oligomerization is nucleic acid sequence-independent, so we expect the roadblock to form at a small number of random sites along the viral genome, as observed *in virio*. Although A3G may bind RT in an RNA-independent interaction[46], a recent report concludes that there is no direct interaction between A3G and RT[31]. In any case, this type of binding is equally probable for any of the 100 RT heterodimers present in the virion[47], and the probability that one of 7 ± 4 A3G molecules binds and inhibits the catalytically active RT molecule is therefore less than 10%. Thus, a possible A3G–RT interaction appears unlikely to be primarily responsible for A3G-induced inhibition of reverse transcription.

The data we present resolve seemingly contradictory mechanisms for A3G inhibition of viral replication by demonstrating that A3G can function as both a fast deaminase and a slow nucleic acid binding protein. Regulation of enzymatic activity via protein oligomerization may be a general property of other APOBEC family members that inhibit replication of retroviruses and retrotransposons independent of deaminase activity. The single-molecule method described here does not require labelling of DNA or protein and is optimal for measuring the biologically important process of slow protein oligomerization on ssDNA.

Methods

A3G preparation and purification. Recombinant WT A3G and A3G FW were expressed in a baculovirus expression system using an *N*-terminal glutathione *S*-transferase (GST) tag and purified. The GST tag was then removed using a Novagen Enterokinase Cleavage Capture Kit. The deaminase activity of purified wild-type A3G was verified using a gel-based uracil DNA glycosylase assay[19] after removal of the GST tag. A similar method was used to verify the enzymatic activity of purified GST-tagged A3G FW. Additional protein preparation details are presented in the Supplementary Methods.

Single-molecule experiments. Biotin-labelled bacteriophage λ DNA was captured between two streptavidin-coated polystyrene beads, one on a fixed micropipette tip and the other held in an optical trap, as described in the Supplementary Methods. The DNA was extended by moving the micropipette tip at a rate of 100 nm s^{-1}, and the resulting force on the bead in the trap was recorded to obtain the force–extension curve for DNA alone. The buffer surrounding the DNA molecule was then exchanged for a solution of fixed protein concentration. Force–extension curves in the presence and absence of protein were fit to the 'Worm-Like Chain' model for dsDNA (Supplementary equation (1)) and the 'Freely-Jointed Chain' model (Supplementary equation (2)) for ssDNA. The A3G-saturated ssDNA force–extension curve was fit to Supplementary equation (4). Measurements of the fraction of ssDNA bound by protein were then determined by fitting force–extension curves to the linear combination of dsDNA extension and A3G-bound ssDNA extension (Supplementary equations (6) and (7)).

Two-step binding model. The kinetics of protein–DNA binding was fit to a two-step binding model, in which it was assumed that an initial fast bimolecular binding event was followed by a slow unimolecular binding event, as described by Supplementary equations (9) to (11), yielding measured fast and slow binding rates k_{fast} and k_{slow} (ref. 48). By then fitting the concentration-dependent measurements of k_{fast} and k_{slow} to the reaction shown in equation (1), we determine the elementary reaction rates for each step k_1, k_{-1}, k_2 and k_{-2}, as well as the elementary equilibrium constants for each step K_1 and K_2, as described in the Supplementary Methods.

Received 7 February 2013; accepted 11 October 2013; published online 24 November 2013

References

1. Malim, M. H. APOBEC proteins and intrinsic resistance to HIV-1 infection. *Philos. Trans. R. Soc. Lond. B* **364,** 675–687 (2009).
2. Harris, R. S. & Liddament, M. T. Retroviral restriction by APOBEC proteins. *Nature Rev. Immunol.* **4,** 868–877 (2004).
3. Duggal, N. K. & Emerman, M. Evolutionary conflicts between viruses and restriction factors shape immunity. *Nature Rev. Immunol.* **12,** 687–695 (2012).
4. Chiu, Y. L. & Greene, W. C. The APOBEC3 cytidine deaminases: an innate defensive network opposing exogenous retroviruses and endogenous retroelements. *Annu. Rev. Immunol.* **26,** 317–353 (2008).
5. Sheehy, A. M., Gaddis, N. C., Choi, J. D. & Malim, M. H. Isolation of a human gene that inhibits HIV-1 infection and is suppressed by the viral Vif protein. *Nature* **418,** 646–650 (2002).
6. Holmes, R. K., Malim, M. H. & Bishop, K. N. APOBEC-mediated viral restriction: not simply editing? *Trends Biochem. Sci.* **32,** 118–128 (2007).
7. Fisher, A. G. *et al.* The *sor* gene of HIV-1 is required for efficient virus transmission *in vitro*. *Science* **237,** 888–893 (1987).
8. Strebel, K. *et al.* The HIV 'A' (sor) gene product is essential for virus infectivity. *Nature* **328,** 728–730 (1987).
9. Goila-Gaur, R. & Strebel, K. HIV-1 Vif, APOBEC, and intrinsic immunity. *Retrovirology* **5,** 1–16 (2008).
10. Lecossier, D., Bouchonnet, F., Clavel, F. & Hance, A. J. Hypermutation of HIV-1 DNA in the absence of the Vif protein. *Science* **300,** 1112 (2003).
11. Mangeat, B. *et al.* Broad antiretroviral defence by human APOBEC3G through lethal editing of nascent reverse transcripts. *Nature* **424,** 99–103 (2003).
12. Zhang, H. *et al.* The cytidine deaminase CEM15 induces hypermutation in newly synthesized HIV-1 DNA. *Nature* **424,** 94–98 (2003).
13. Suspène, R. *et al.* APOBEC3G is a single-stranded DNA cytidine deaminase and functions independently of HIV reverse transcriptase. *Nucleic Acids Res.* **32,** 2421–2429 (2004).
14. Yu, Q. *et al.* Single-strand specificity of APOBEC3G accounts for minus-strand deamination of the HIV genome. *Nature Struct. Mol. Biol.* **11,** 435–442 (2004).
15. Harris, R. S. *et al.* DNA deamination mediates innate immunity to retroviral infection. *Cell* **113,** 803–809 (2003); erratum **116,** 629 (2004).
16. Levin, J. G., Mitra, M., Mascarenhas, A. & Musier-Forsyth, K. Role of HIV-1 nucleocapsid protein in HIV-1 reverse transcription. *RNA Biol.* **7,** 754–774 (2010).
17. Newman, E. N. C. *et al.* Antiviral function of APOBEC3G can be dissociated from cytidine deaminase activity. *Curr. Biol.* **15,** 166–170 (2005).
18. Holmes, R. K., Koning, F. A., Bishop, K. N. & Malim, M. H. APOBEC3F can inhibit the accumulation of HIV-1 reverse transcription products in the absence of hypermutation—comparisons with APOBEC3G. *J. Biol. Chem.* **282,** 2587–2595 (2007).
19. Iwatani, Y., Takeuchi, H., Strebel, K. & Levin, J. G. Biochemical activities of highly purified, catalytically active human APOBEC3G: correlation with antiviral effect. *J. Virol.* **80,** 5992–6002 (2006).
20. Luo, K. *et al.* Cytidine deaminases APOBEC3G and APOBEC3F interact with human immunodeficiency virus type 1 integrase and inhibit proviral DNA formation. *J .Virol.* **81,** 7238–7248 (2007).
21. Turelli, P., Mangeat, B., Jost, S., Vianin, S. & Trono, D. Inhibition of hepatitis B virus replication by APOBEC3G. *Science* **303,** 1829 (2004).
22. Bogerd, H. P., Wiegand, H. L., Doehle, B. P., Lueders, K. K. & Cullen, B. R. APOBEC3A and APOBEC3B are potent inhibitors of LTR-retrotransposon function in human cells. *Nucleic Acids Res.* **34,** 89–95 (2006).
23. Bogerd, H. P. *et al.* Cellular inhibitors of long interspersed element 1 and Alu retrotransposition. *Proc. Natl Acad. Sci. USA* **103,** 8780–8785 (2006).
24. Chen, H. *et al.* APOBEC3A is a potent inhibitor of adeno-associated virus and retrotransposons. *Curr. Biol.* **16,** 480–485 (2006).
25. Muckenfuss, H. *et al.* APOBEC3 proteins inhibit human LINE-1 retrotransposition. *J. Biol. Chem.* **281,** 22161–22172 (2006).
26. Kinomoto, M. *et al.* All APOBEC3 family proteins differentially inhibit LINE-1 retrotransposition. *Nucleic Acids Res.* **35,** 2955–2964 (2007).
27. Niewiadomska, A. M. *et al.* Differential inhibition of long interspersed element 1 by APOBEC3 does not correlate with high-molecular-mass-complex formation or P-body association. *J. Virol.* **81,** 9577–9583 (2007).
28. Bulliard, Y. *et al.* Structure–function analyses point to a polynucleotide-accommodating groove essential for APOBEC3A restriction activities. *J .Virol.* **85,** 1765–1776 (2011).
29. Narvaiza, I. *et al.* Deaminase-independent inhibition of parvoviruses by the APOBEC3A cytidine deaminase. *PLoS Pathog.* **5,** e1000439 (2009).
30. Bishop, K. N., Verma, M., Kim, E. Y., Wolinsky, S. M. & Malim, M. H. APOBEC3G inhibits elongation of HIV-1 reverse transcripts. *PLoS Pathog.* **4,** e1000231 (2008).
31. Adolph, M. B., Webb, J. & Chelico, L. Retroviral restriction factor APOBEC3G delays the initiation of DNA synthesis by HIV-1 reverse transcriptase. *Plos One* **8,** e64196 (2013).
32. Iwatani, Y. *et al.* Deaminase-independent inhibition of HIV-1 reverse transcription by APOBEC3G. *Nucleic Acids Res.* **35,** 7096–7108 (2007).
33. Li, X. Y., Guo, F., Zhang, L. & Kleiman, L. & Cen S. APOBEC3G inhibits DNA strand transfer during HIV-1 reverse transcription. *J. Biol. Chem.* **282,** 32065–32074 (2007).
34. Mbisa, J. L. *et al.* Human immunodeficiency virus type 1 cDNAs produced in the presence of APOBEC3G exhibit defects in plus-strand DNA transfer and integration. *J. Virol.* **81,** 7099–7110 (2007).
35. Gillick, K. *et al.* Suppression of HIV-1 infection by APOBEC3 proteins in primary human CD4+ T cells is associated with inhibition of processive reverse transcription as well as excessive cytidine deamination. *J. Virol.* **87,** 1508–1517 (2013).
36. Xu, H. Z. *et al.* Stoichiometry of the antiviral protein APOBEC3G in HIV-1 virions. *Virology* **360,** 247–256 (2007).
37. Chelico, L., Sacho, E. J., Erie, D. A. & Goodman, M. F. A model for oligomeric regulation of APOBEC3G cytosine deaminase-dependent restriction of HIV. *J. Biol. Chem.* **283,** 13780–13791 (2008).
38. Nowarski, R., Britan-Rosich, E., Shiloach, T. & Kotler, M. Hypermutation by intersegmental transfer of APOBEC3G cytidine deaminase. *Nature Struct. Mol. Biol.* **15,** 1059–1066 (2008).
39. King, G. A. *et al.* Revealing the competition between peeled ssDNA, melting bubbles, and S-DNA during DNA overstretching using fluorescence microscopy. *Proc. Natl Acad. Sci. USA* **110,** 3859–3864 (2013).
40. Chaurasiya, K. R., Paramanathan, T., McCauley, M. J. & Williams, M. C. Biophysical characterization of DNA binding from single molecule force measurements. *Phys. Life Rev.* **7,** 299–341 (2010).
41. Senavirathne, G. *et al.* Single-stranded DNA scanning and deamination by APOBEC3G cytidine deaminase at single molecule resolution. *J. Biol. Chem.* **287,** 15826–15835 (2012).
42. Chelico, L., Prochnow, C., Erie, D. A., Chen, X. S. & Goodman, M. F. Structural model for deoxycytidine deamination mechanisms of the HIV-1 inactivation enzyme APOBEC3G. *J. Biol. Chem.* **285,** 16195–16205 (2010).
43. Huthoff, H., Autore, F., Gallois-Montbrun, S., Fraternali, F. & Malim, M. H. RNA-dependent oligomerization of APOBEC3G is required for restriction of HIV-1. *PLoS Pathog.* **5,** e1000330 (2009).
44. Bélanger, K., Savoie, M., Rosales Gerpe, M. C., Couture, J-F. & Langlois, M-A. Binding of RNA by APOBEC3G controls deamination-independent restriction of retroviruses. *Nucleic Acids Res.* **41,** 7438–7452 (2013).
45. Soros, V. & Greene, W. APOBEC3G and HIV-1: strike and counterstrike. *Curr. HIV/AIDS Rep.* **4,** 3–9 (2007).
46. Wang, X. X. *et al.* The cellular antiviral protein APOBEC3G interacts with HIV-1 reverse transcriptase and inhibits its function during viral replication. *J. Virol.* **86,** 3777–3786 (2012).
47. Coffin, J. M., Hughes, S. H. & Varmus, H. E. *Retroviruses* (Cold Spring Harbor Laboratory Press, 1997).
48. Vo, M. N., Barany, G., Rouzina, I. & Musier-Forsyth, K. Mechanistic studies of mini-TAR RNA/DNA annealing in the absence and presence of HIV-1 nucleocapsid protein. *J. Mol. Biol.* **363,** 244–261 (2006).

Acknowledgements

The authors thank D. Pollpeter, M.H. Malim and D. Rueda for valuable discussions, and M.F. Goodman for his generous gift of the F126A/W127A mutant clone. This work was supported in part by the National Institutes of Health (GM072462 to M.C.W. and GM065056 to K.M-F.) and the National Science Foundation (MCB-1243883 to M.C.W.), the Japan Society for the Promotion of Science (JSPS; KAKENHI_24590568 to Y.I.), and in part by funds from the NIH Intramural Research Program (NICHD; to J.G.L.). K.R.C. was supported by the NSF IGERT Program (DGE-0504331).

Author contributions

M.C.W., K.R.C. and I.R. designed the experiments. K.R.C. performed experiments and analysed the data. M.M. performed experiments with the mutant. H.G. performed preliminary experiments. S.K., W.W., D.F.Q., T.W., Y.I., D.S.B.C. and A.H. prepared the proteins. I.R. developed the binding model. K.R.C., M.C.W., I.R., J.G.L. and K.M-F. wrote the manuscript.

Additional information

Supplementary information is available in the online version of the paper. Reprints and permissions information is available online at www.nature.com/reprints. Correspondence and requests for materials should be addressed to M.C.W.

Competing financial interests

The authors declare no competing financial interests.

OPEN ACCESS Freely available online

PLOS | ONE

APOBEC3G Oligomerization Is Associated with the Inhibition of Both *Alu* and LINE-1 Retrotransposition

Takayoshi Koyama[1☯], Juan Fernando Arias[1☯], Yukie Iwabu[1], Masaru Yokoyama[2], Hideaki Fujita[3], Hironori Sato[2], Kenzo Tokunaga[1*]

1 Department of Pathology, National Institute of Infectious Diseases, Tokyo, Japan, **2** Pathogen Genomics Center, National Institute of Infectious Diseases, Tokyo, Japan, **3** Faculty of Pharmaceutical Sciences, Nagasaki International University, Nagasaki, Japan

Abstract

Alu and LINE-1 (L1), which constitute ~11% and ~17% of the human genome, respectively, are transposable non-LTR retroelements. They transpose not only in germ cells but also in somatic cells, occasionally causing cancer. We have previously demonstrated that antiretroviral restriction factors, human APOBEC3 (hA3) proteins (A–H), differentially inhibit L1 retrotransposition. In this present study, we found that hA3 members also restrict *Alu* retrotransposition at differential levels that correlate with those observed previously for L1 inhibition. Through deletion analyses based on the best-characterized hA3 member human APOBEC3G (hA3G), its N-terminal 30 amino acids were required for its inhibitory activity against *Alu* retrotransposition. The inhibitory effect of hA3G on *Alu* retrotransposition was associated with its oligomerization that was affected by the deletion of its N-terminal 30 amino acids. Through structural modeling, the amino acids 24 to 28 of hA3G were predicted to be located at the interface of the dimer. The mutation of these residues resulted in abrogated hA3G oligomerization, and consistently abolished the inhibitory activity of hA3G against *Alu* retrotransposition. Importantly, the anti-L1 activity of hA3G was also associated with hA3G oligomerization. These results suggest that the inhibitory activities of hA3G against *Alu* and L1 retrotransposition might involve a common mechanism.

Citation: Koyama T, Arias JF, Iwabu Y, Yokoyama M, Fujita H, et al. (2013) APOBEC3G Oligomerization Is Associated with the Inhibition of Both *Alu* and LINE-1 Retrotransposition. PLoS ONE 8(12): e84228. doi:10.1371/journal.pone.0084228

Editor: Chen Liang, Lady Davis Institute for Medical Research, Canada

Received October 23, 2013; **Accepted** November 20, 2013; **Published** December 19, 2013

Funding: This work was supported by grants from the Ministry of Health, Labor and Welfare of Japan (Research on HIV/AIDS project no.H24-005, H24-008 and H25-010), and from the Ministry of Education, Science, Technology, Sports and Culture of Japan (22590428). The funders had no role in study design, data collection and analysis, decision to publish, or preparation of the manuscript.

Competing interests: The authors have declared that no competing interests exist.

* Email: tokunaga@nih.go.jp

☯ These authors contributed equally to this work.

Introduction

Retrotransposons compose ~42% of the human genome, and these elements are classified into the non-LTR and LTR classes. Non-LTR retrotransposons are subdivided into long interspersed elements (LINEs) and short interspersed elements (SINEs), representatives of which are LINE-1 (L1) and *Alu*, which comprise ~17% and ~11% of the human genome, respectively [1]. L1 elements harbor two ORFs: ORF1, which encodes an RNA-binding protein, and ORF2, which encodes an endonuclease-like and reverse transcriptase-like protein. After translation, these proteins bind to the L1 RNA to form a ribonucleoprotein particle that is imported into the nucleus to be integrated into the genome through target-primed reverse transcription [2-4]. Unlike L1, *Alu* elements do not encode a reverse transcriptase or an endonuclease; rather, the transcribed *Alu* RNAs hijack the L1-encoded enzymes to move to new locations in the genome through mechanisms that are as yet unclear [5]. Importantly, retrotransposition by L1 and *Alu* occurs not only in germ cells, causing several genetic diseases [6-13], but also in somatic cells, such as brain tissues [14,15], and malignant tissues and cells such as B-cell lymphoma cells [16], breast carcinoma tissue [17], colon carcinoma tissue [18], and hepatocellular carcinoma tissue [19]. These facts indicate that an intrinsic protection system should function properly to suppress these types of retrotransposition in normal somatic cells.

Human APOBEC3G (hA3G) is one of the seven members of the APOBEC3 (hA3) family of cytidine deaminases (hA3A to hA3H). hA3G is known to be an intrinsic retroviral restriction factor that inhibits Vif-defective human immunodeficiency virus type 1 (HIV-1) infection by being incorporated into viral particles and mediating extensive deamination of the nascent minus-strand viral DNA during reverse transcription, which results in G-to-A hypermutation [20-23]. This antiretroviral restriction extends to not only exogenous retroviruses, such as

simian immunodeficiency virus [24-27], primate foamy virus [28,29], human T-cell leukemia virus type I [30], murine leukemia virus [21,26,31], mouse mammary tumor virus [32], and equine infectious anemia virus [22] , but also endogenous retroelements, such as the MusD and intracisternal A-particle LTR murine retrotransposons and, as described below, human *Alu* and L1 retrotransposons ([33-40]; see also review in ref[41].). hA3G also restricts infection by hepatitis B virus, which replicates its DNA genome by reverse transcription of an RNA intermediate [42,43]. Whereas pre-primate mammals encode one, two to three A3 proteins [44], primates have acquired seven different A3 genes through 33 million years of evolution [45]. Such expansion of the hA3 genes correlates with an abrupt reduction in retrotransposition activity in primates, suggesting that these proteins have evolved to protect hosts from the genomic instability caused by retroelements [46].

We previously reported that hA3 family proteins have differential levels of anti-L1 activity that do not correlate with either antiretroviral activity or subcellular localization patterns [37]. Although several groups that performed similar studies showed that hA3G has little or no anti-L1 activity [47-50], we and others have found that the hA3G is indeed able, albeit less potently than hA3A or hA3B, to restrict L1 retrotransposition [37-40]. Such discrepancies might be attributed to the cell-type-dependent expression levels of hA3G, as we previously demonstrated [37]. We also found that hA3G inhibits L1 retrotransposition independently of its deaminase activity, which is primarily required for its antiretroviral function, and hA3G likely prevents L1 DNA synthesis *per se* [37]. With regard to the inhibition of *Alu* by hA3 family members, several groups have reported that hA3A, hA3B [49], hA3G [34-36], hA3DE, and hA3H [51] inhibit *Alu* retrotransposition. In this study, we found that all hA3 family members, from hA3A to hA3H, are able to inhibit *Alu* retrotransposition. The inhibitory effect of hA3G on *Alu* retrotransposon was associated with the N-terminal 30 amino acid residues and with hA3G's oligomerization activity, but not with its deaminase activity. Structural modeling showed that amino acid positions 24–28 are responsible for the oligomerization of hA3G. This result was verified by immunoprecipitation using an hA3G mutant with amino acid substitutions at these positions. Consistent with this result, we found that amino acid positions 24–28 of hA3G are critical for its inhibitory activity against *Alu* retrotransposon. Importantly, these amino acids were also shown to be important for L1 inhibition, suggesting that both *Alu* and L1 retrotransposition might be restricted by similar mechanisms involving hA3G, which require the oligomerization of this restriction factor.

Materials and Methods

DNA constructs

The hemagglutinin (HA)-tagged hA3 expression plasmids (phA3A-HA, phA3B-HA, phA3C-HA, phA3DE-HA, phA3F-HA, phA3G-HA, and phA3H-HA), the GFP expression plasmid pCA-EGFP, the empty expression vector pCAGGS-HA, the L1 indicator construct pCEP4/L1mneoI/ColE1 (kindly provided by N. Gilbert), the L1 ORF2 expression plasmid pBudORF2opt (kindly provided by A.M. Roy-Engel), the *Alu* indicator construct pYa5neotet (kindly provided by T. Heidmann), Vif-deficient HIV-1 proviral indicator construct pNLLuc-F(-)E(-), and VSV-G expression plasmid pHIT/G have previously been described elsewhere [5,37,52-55] (note that the hA3h expression plasmid encodes the haplotype I). The myc-tagged version of the wild-type hA3G expression plasmid, phA3G-myc, was also created. A series of N-terminal deletion mutants of hA3G (phA3G-NΔ30-HA, -NΔ60-HA, -NΔ90-HA, -NΔ120-HA, and -NΔ150-HA) were created by inserting serially deleted PCR fragments of hA3G into the mammalian expression plasmid pCAGGS with a C-terminal HA-tag. The deaminase-deficient mutant (phA3G-E259Q-HA), the oligomerization-deficient mutant (phA3G-C97/100A-HA), and the N-terminal mutants (phA3G-5G(24–28)-HA, phA3G-4G(124–127)-HA, phA3G-R24G-HA, and phA3G-Y125G-HA) of hA3G were created using phA3G-HA as a template with a QuikChange site-directed mutagenesis kit (Stratagene).

Cell maintenance, transfections, and protein analyses

HeLa and 293T cells were maintained under standard conditions. 293T cells were transfected with HA-tagged hA3 wild-type and mutant plasmids using the FuGENE 6 transfection reagent (Roche Applied Science) according to the manufacturer's instructions. Cell extracts from transfected cells were subjected to gel electrophoresis and then transferred to a nitrocellulose membrane. The membranes were probed with an anti-HA mouse monoclonal antibody (Sigma). The antibody-bound proteins were visualized to confirm hA3 protein expression by chemiluminescence using an ECL Western blotting detection system (GE Healthcare) and an LAS-3000 imaging system (FujiFilm).

Immunofluorescence microscopy

HeLa cells were plated on 13-mm glass coverslips and transfected with 0.5 μg of hA3 expressing plasmids by using FUGENE6. The transfected cells were fixed with 4% paraformaldehyde at room temperature for 30 min, permeabilized with 0.05% saponin for 10 min, and immunostained with an anti-HA monoclonal antibody (5 μg/ml). The secondary goat anti-mouse antibody that was conjugated with Cy3 was used at 5 μg/ml. All immunofluorescence images were observed on a Leica DMRB microscope (Wetzlar, Germany) equipped with a 63×1.32 NA oil immersion lens (PL APO), acquired through a cooled CCD camera, MicroMAX (Princeton Instruments, Trenton, NJ), and digitally processed using IPlab Software (Scanalytics, Fairfax, VA). All images were assembled using Adobe Photoshop (Adobe Systems, Mountain View, CA).

L1 and Alu retrotransposition assay

L1 and *Alu* retrotransposition assays were performed by co-transfecting 2 x 10^5 HeLa cells with 0.1 μg of the respective hA3 expression plasmid (or a mock expression vector, pCAGGS-HA, as a positive control) together with either 0.3 μg of the neomycin-resistance (neo^r)-based L1 expression vector pCEP4/L1mneoI/ColE1 and 0.1 μg of an empty vector (for the

L1 retrotransposition assay) or 0.3 μg of the neo^r-based *Alu* expression vector pYa5neotet and 0.1 μg of the L1 ORF2 expression plasmid pBudORF2opt (for the *Alu* retrotransposition assay) using Lipofectamine and Plus reagents (Invitrogen). As a negative control, 0.5 μg of a GFP expression vector, pCA-EGFP, was transfected into HeLa cells. After 72 h, the cells were trypsinized, re-seeded into T25 or T75 flasks for G418 selection (1 mg/ml for the L1 assay and 400 μg/ml for the *Alu* assay), and maintained. At 14 days after selection, the resultant G418-resistant (G418^R) colonies were fixed, stained with crystal violet (Merck), and counted.

Oligomerization assay

To perform a coimmunoprecipitation-based oligomerization assay, plasmids (0.5 μg) expressing HA-tagged wild-type and mutant hA3G were transfected along with phA3G-myc (0.5 μg) into 293T cells using FuGENE 6. After 48 h, the transfected cells were suspended in 500 μl of RIPA buffer (50 mM Tris-HCl, pH 7.4, 150 mM NaCl, 1% NP-40, 0.5% sodium deoxycholate, 0.1% SDS, complete protease inhibitor cocktail [Roche]). The resultant lysates were clarified by brief centrifugation, pre-cleared with 30 μl of Protein A-Agarose Fast Flow (GE Healthcare) for 1 h at 4°C, and then incubated with an anti-myc affinity gel (Sigma). After 1 h at 4°C, the immune complexes were extensively washed with RIPA buffer. Equal aliquots of the total and bound fractions were subjected to gel electrophoresis and transferred to a nitrocellulose membrane. The membranes were probed with an anti-HA mouse monoclonal antibody (Sigma) or an anti-β-actin mouse monoclonal antibody (AC-74, Sigma). The signal intensities of the immunoprecipitated hA3G protein on Western blots were quantified using the LAS-3000 imaging system (Fujifilm). For the RNase A treatment experiment, the immune complexes were separated into two aliquots. The wild-type sample was incubated with or without 25 U of RNase A (Sigma) at room temperature for 30 min. Samples were extensively washed and then resuspended in loading dye. The samples were assayed as described above.

Molecular modeling of the head-to-head dimer structure of the N-terminus of hA3G

Head-to-head dimer models of hA3G N-terminal domain were obtained by homology modelling using either the crystal structure of human APOBEC2 (hA2) at a resolution of 2.50 Å or the NMR structure of the C-terminal domain of hA3G (PDB code: 2NYT chain A [56] or 2JYW [57], respectively) as a template, as previously performed [34,58-60]. To minimize misalignments between the hA3G N-terminal domain as a target sequence and either hA2 or the C-terminal domain of hA3G as a template sequence, we used the multiple sequence alignment method with the sequences of hA3A (GenBank accession number: NM_145699), hA3C (GenBank accession number: NM_014508), and hA3F (GenBank accession number: NM_145298). Multiple sequence alignments were generated using 'MOE-Align' in Molecular Operating Environment (MOE) version 2010.10 (Chemical Computing Group Inc., Quebec, Canada). Three-dimensional (3-D) models of the hA3G N-terminal domain were constructed by the homology modeling technique using 'MOE-Homology' in MOE as previously described [61]. We obtained 25 intermediate models per homology modeling session in MOE, and we selected the 3-D models that were intermediate models with best scores according to the generalized Born/volume integral methodology [62]. The 3-D structure was thermodynamically optimized by energy minimization using MOE and an AMBER99 force field [63] combined with the generalized Born model of aqueous solvation implemented in MOE [64]. The physically unacceptable local structure of the optimized 3-D model was further refined based on the evaluation of the Ramachandran plot using MOE.

Results

hA3 family members differentially inhibit Alu retrotransposition

To determine if hA3 family members are able to inhibit *Alu* retrotransposition as well as L1 retrotransposition [37], we performed a neo^r-based retrotransposition assay [5]. In this assay system, we utilized a L1 ORF2 expression plasmid that is required for *Alu* retrotransposition [53], together with an *Alu* clone DNA carrying a reverse-oriented neo^r gene separated by a gamma-globin intron. After transfection of the cells with this construct, neo^r with *Alu* is transcribed, spliced, reverse-transcribed, and integrated. Then, the neo^r gene that is integrated with *Alu* is driven by the CMV promoter and expressed. After G418 selection following transfection, we were able to quantify the retrotransposition level by counting the number of G418^R colonies. hA3 protein expression in the cells were confirmed by immunoblotting using anti-HA antibodies (Figure 1A). Without the co-expression of an hA3 protein, *Alu* retrotransposition occurred at the level shown in the upper left panel of Figure 1B. In contrast, the co-expression of any of the hA3 proteins differentially inhibited *Alu* retrotransposition, and in particular, the expression of hA3A, hA3B, or hA3G strongly decreased the transposition level of *Alu* elements (Figure 1C). Thus, we conclude that hA3 proteins act to differentially suppress *Alu* retrotransposition. Importantly, in agreement with previous reports [34-36,39], we observed that hA3G has an inhibitory effect on *Alu* retrotransposition in the assay. It should be noted that these activities against *Alu* correlated exactly with the patterns previously observed for the inhibition of L1 [37].

The *N*-terminal 30 amino acids of hA3G determine the inhibitory effect on Alu retrotransposition

Because hA3G is the best characterized hA3 family member protein, we focused on this protein and attempted to determine the region responsible for its anti-retrotransposon activities. To identify the relevant region, we created a series of mutants with serial deletions from the N-terminus up to amino residue 150 (Figure 2A). Protein expression in the cells transfected with each plasmid was confirmed by immunoblotting using an anti-HA antibody (Figure 2B). hA3G mutants lacking the C-terminal domain were undetectable as previously reported [34,65] and therefore could not be used for further experiments. Immunofluorescence microscopy confirmed that hA3G deletion

Oligomerized hA3G inhibits retrotransposition

Figure 1

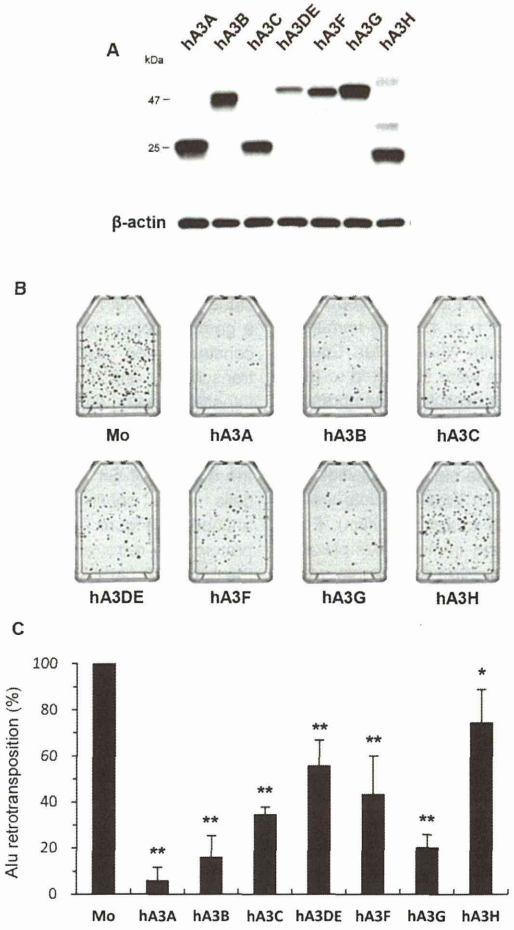

Figure 1. hA3 proteins inhibit Alu retrotransposition at differential levels. (**A**) Western blot analysis was performed by using extracts from 293T cells transfected with HA-tagged hA3 expression plasmids. Antibodies specific for HA were used. (**B**, **C**) HeLa cells were cotransfected with the *neo*'-based *Alu* expression vector pYa5neotet and the L1 ORF2 expression plasmid pBudORF2opt, together with the respective hA3 expression plasmid. Seventy-two hours later, the cells were trypsinized, re-seeded into T25 or T75 flasks, and subjected to G418 (400 μg/ml) selection. At 14 days after selection, the resultant $G418^R$ colonies fixed, stained with crystal violet (B), and counted to determine the level of *Alu* retrotransposition (C). The retrotransposition level in the absence of hA3 proteins was set to 100%. The data shown are the mean ± SD of triplicate experiments. Mo, mock. $^*P < 0.05$, $^{**}P < 0.005$, *t*-test.

doi: 10.1371/journal.pone.0084228.g001

mutant proteins other than NΔ150 were predominantly localized to the cytoplasm, as was the wild-type protein (Figure 2C). These deletions also abrogated the anti-HIV-1 activity of hA3G (Figure S1). We performed an *Alu* retrotransposition assay by transfecting HeLa cells with the *Alu* expression plasmid, the L1 expression plasmid, and a wild-type or mutant hA3G plasmid, and we observed that the deletion of 30 or more residues from the N-terminus of hA3G completely abrogated the inhibitory activity of hA3G on *Alu* retrotransposition (Figures 2D and 2E). We therefore conclude that the N-terminal 30 amino acids of hA3G are critical for the inhibition of *Alu* retrotransposition.

The inhibitory effect of hA3G on Alu retrotransposition is associated with its oligomerization and is independent of its deaminase activity

The anti-HIV-1 activity of hA3G is known to be dependent on two different activities, deamination and oligomerization, the former of which has been shown to be disrupted by the mutation of E259 located in the C-terminal cytidine deaminase (CD2) [65,66], and the latter of which has been reported to be abrogated by the mutation of C97 and C100 located in the N-terminal cytidine deaminase (CD1) [65]. Based on these past findings, we wished to determine which functions of hA3G are crucial for blocking the ability of *Alu* to retrotranspose. We created plasmids expressing hA3G defective in either oligomerization or deamination (C97/100A or E259Q, respectively; Figure 3A) and confirmed the expression of these proteins by immunoblotting using an anti-HA antibody (Figure 3B). Interestingly, the *Alu* retrotransposition assay revealed that the C97/100A oligomerization mutant of hA3G had no inhibitory activity against *Alu* retrotransposition, whereas the E259Q deamination mutant retained wild-type activity (Figure 3C). These observations confirmed the previous results [34,35], showing that the inhibition of *Alu* retrotransposition by hA3G is not due to the ability of hA3G to deaminate this retrotransposon but is due to its ability to form an oligomer.

The *N*-terminal 30 amino acids of hA3G are required for the oligomerization of this protein

Because hA3G's inhibitory activity against *Alu* retrotransposition was abolished in the mutants carrying an N-terminal deletion of 30 or more residues (Figure 2) and in the oligomerization mutant harboring mutations at amino acid positions 97 and 100 (Figure 3), we reasoned that the N-terminal 30 amino acids of hA3G might be critical for its ability to form oligomers. To test this hypothesis, we performed an oligomerization assay by coexpressing wild-type hA3G tagged with Myc and the mutant hA3Gs tagged with HA. The cell lysates were then immunoprecipitated with an anti-HA antibody and immunoblotted with an anti-Myc antibody. As shown in Figure 4, the E259Q deamination mutant of myc-tagged hA3G was efficiently coimmunoprecipitated with the HA-tagged wild-type protein. In contrast, the N-terminal serial deletion mutants lacking 30 or more residues completely lost the ability to oligomerize, as did the C97/100A mutant. When the immunoprecipitated samples were treated with RNase A, the oligomerization efficiency of hA3G was moderately decreased (Figure S2), consistent with the previous reports that cellular RNA might contribute to the stabilization of hA3G's oligomer [34]. Thus, the 30 amino acids at the N-terminus of hA3G are responsible for its oligomerization.

The *N*-terminal 30 amino acids of hA3G are the structural key for its oligomerization

To fully understand the mechanism by which N-terminal 30 amino acids of hA3G regulate oligomerization, we analyzed the effect of the deletion of the N-terminal 30 amino acids on the predicted 3-D structure of the hA3G dimer that was reported to be the major form of hA3G oligomer [34,59]. Thermodynamically stable N-terminal structures of wild-type hA3G and its N-terminal 30-amino-acid deletion mutant were constructed by homology modeling using the hA2 crystal structure as a template. As shown in Figures 5A and B, when the structures of the wild-type and deletion mutant hA3G proteins were compared, it was obvious that the N-terminal 30 amino acids (shown in cyan in Figure 5A) were present along the contact surface of the hA3G dimer, and therefore, the deletion of this region could abolish the interaction interface between the two hA3G molecules. We thus conclude that the N-terminal 30 amino acid residues of hA3G are located at the dimer interface and are critical for oligomerization.

Residues 24–28 contribute to the ability of hA3G to homooligomerize and inhibit Alu retrotransposition

Next, we analyzed the interaction interface of the hA3G dimer by structural modeling based not only on the hA2 crystal structure but also on the C-terminal hA3G (hA3G-C) NMR structure in parallel. Both structural modeling of wild-type hA3G revealed that, among the N-terminal 30 amino acids, a cluster of dimer interface residues (R24, P25, I26, L27, and S28) located in the N-terminal core structure α1-loop-β1 of hA3G interact with the counterpart residues of another monomer (Figures 6A and 6B). Importantly, this interface corresponds structurally (but not genetically) to a part of the potential oligomerization interfaces of the hA3G C-terminal domain, as described by Shandilya et al. [67]. At this putative interaction surface (Figures 6A and 6B), R24 likely interacts with D130 of another monomer through hydrogen bonds and electrostatic interactions, whereas the isoleucine/leucine residues at positions 26/27 can form a hydrophobic interaction with the counterpart residues of another monomer. hA2-based modeling shows that the serine residue at position 28 forms another hydrogen bond with the counterpart residues of another monomer (Figure 6A), although the same residue in hA3G-C-based modeling appears to be slightly separated from the counterpart residue of another monomer (Figure 6B). Additionally, the structural stability would be enhanced by a proline residue at position 25 in the loop. Thus, we speculated that the mutation of these residues might abolish the oligomerization of hA3G. To test this hypothesis, we first addressed whether structural modeling would be able to distinguish oligomerization-deficient and oligomerization-intact hA3Gs by analyzing the model of an hA3G mutant (hA3G-4G(124–127)), in which we introduced the small amino acid glycine in place of the aromatic amino acid residues

Figure 2

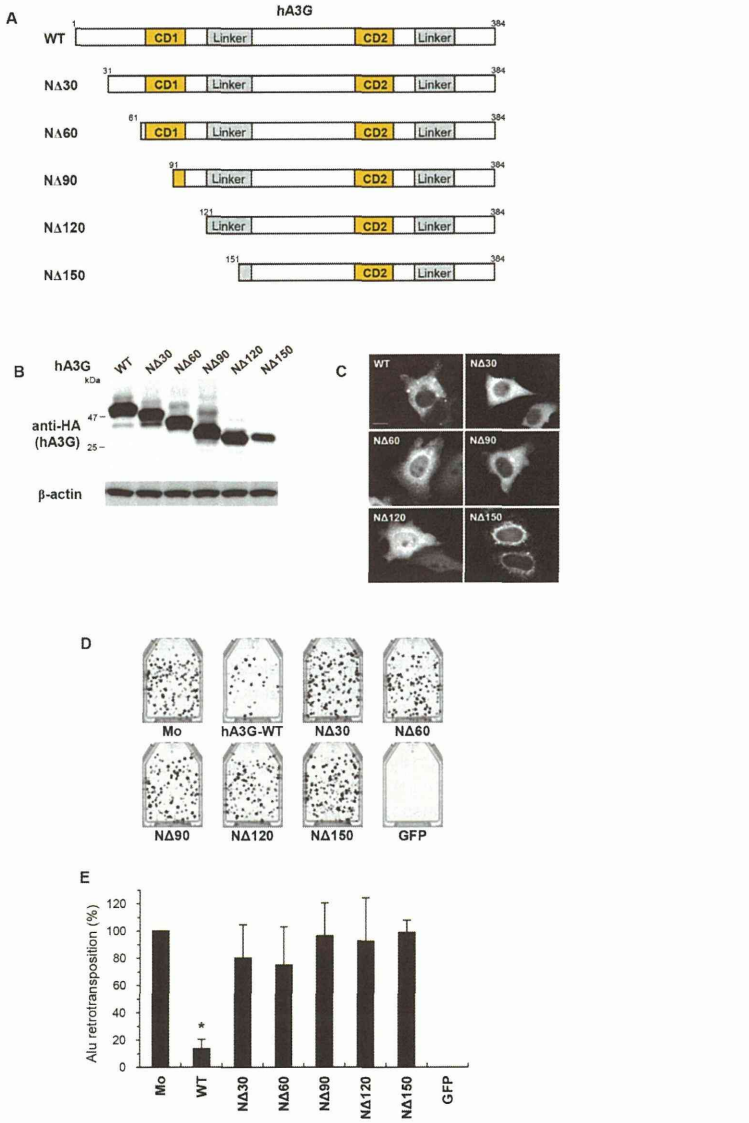

Figure 2. The N-terminal 30 amino acids regulate the anti-Alu activity of hA3G. (**A**) Schematic depiction of a series of N-terminal deletion mutants of hA3G. CD1, N-terminal cytidine deaminase; CD2, C-terminal cytidine deaminase. (**B**) Western blot analysis was performed using extracts from 293T cells transfected with plasmids expressing HA-tagged hA3G mutant proteins. Monoclonal antibodies specific for HA (upper) or β-actin (lower) were used. (**C**) Representative images of HeLa cells transfected with the indicated plasmids are shown. hA3G wild-type (WT), NΔ30, NΔ60, NΔ90, and NΔ120 mutant proteins were predominantly localized to the cytoplasm, whereas NΔ150 mutant protein localized to the perinuclear region. Scale bar: 20 μm. (**D**, **E**) An *Alu* retrotransposition assay was performed as described in Figure 1. Crystal violet-stained G418^R colonies were counted to determine the level of *Alu* retrotransposition. The data shown are the mean ± SD of triplicate experiments. Mo, mock; WT, wild-type hA3G; GFP, GFP only. *$P < 0.005$, *t*-test.

doi: 10.1371/journal.pone.0084228.g002

Oligomerized hA3G inhibits retrotransposition

Figure 3

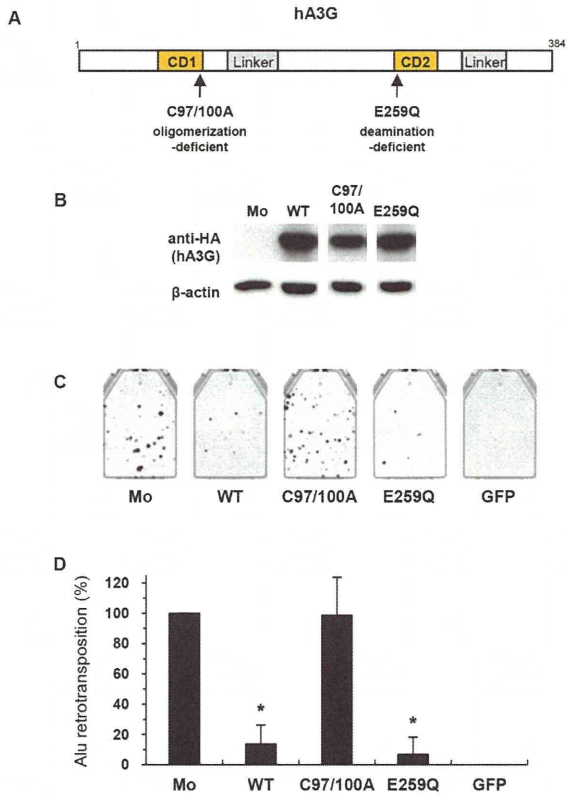

Figure 3. The anti-Alu activity of hA3G is associated with its oligomerization and is independent of its deaminase activity. (**A**) Schematic depiction of two mutants: an oligomerization-deficient mutant, C97/100A, and a deamination-deficient mutant, E259Q. (**B**) Western blot analysis was performed using extracts from 293T cells transfected with plasmids expressing HA-tagged hA3G mutant proteins. Monoclonal antibodies specific for HA (upper) or β-actin (lower) were used. (**C**, **D**) An *Alu* retrotransposition assay was performed as described in Figure 1. A GFP expression vector was used as a negative control. Crystal violet-stained $G418^R$ colonies were counted to determine the level of *Alu* retrotransposition. The data shown are the mean ± SD of triplicate experiments. Mo, mock; WT, wild-type hA3G; GFP, GFP only. $^*P < 0.005$, *t*-test.

doi: 10.1371/journal.pone.0084228.g003

(Y124, Y125, F126, and W127) that have been predicted to be hot spots of protein–protein interaction [68] and have been reported to be critical for the RNA-mediated oligomerization of hA3G [34,59]. The structural model of hA3G-4G(124–127) indicates that the mutant does not form the aromatic cluster, leaving a prominent space between two monomers (compare

Oligomerized hA3G inhibits retrotransposition

Figure 4

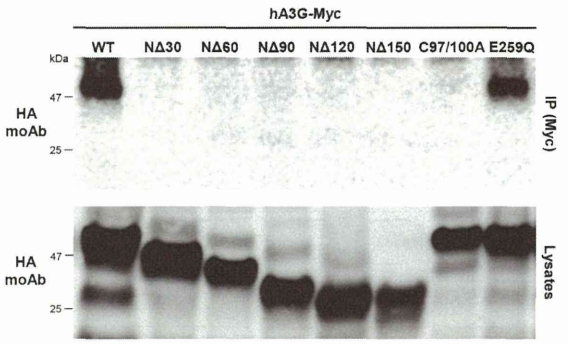

Figure 4. The homooligomerization of hA3G is dependent on the N-terminal 30 amino acid residues of this protein. 293T cells cotransfected with the Myc-tagged and HA-tagged hA3G expression plasmids were immunoprecipitated (IP) with an anti-Myc polyclonal antibody. The resulting complexes were analyzed by immunoblotting with a monoclonal antibody against the HA tag to detect oligomerized hA3G (upper). Cell lysate aliquots were also analyzed in parallel by immunoblotting for the HA tag (lower). WT, wild-type hA3G.

doi: 10.1371/journal.pone.0084228.g004

the left and right panels of Figure 6C and the left and right panels of Figure 6D). Given this result, we then introduced in silico mutations into the five-amino-acid cluster (R24, P25, I26, L27, and S28) of the putative dimer interface (RPILS –> GGGGG; designated 5G(24–28)) (compare the left and right panels of Figure 6E and the left and right panels of Figure 6F). The space between the two monomers of the mutant was clearly comparable to that of 4G(124–127), implying that the 5G(24–28) mutant cannot form a dimer. Based on the structural models, we constructed the myc-tagged N-terminal mutants hA3G-5G(24–28) and hA3G-4G(124–127) to determine whether the former hA3G mutant is unable to physically oligomerize. To assess oligomerization, we performed coimmunoprecipitation-based oligomerization assays using wild-type and mutant hA3G proteins. The 5G(24–28) mutant was not coimmunoprecipitated (Figure 6G), nor was 4G(124–127), suggesting that these mutants do not have the ability to oligomerize. Finally, to determine whether the 4G(124–127) and 5G(24–28) mutants lacks anti-*Alu* activity, we performed the retrotransposition assay and found out that these mutants had completely lost the ability to inhibit *Alu* retrotransposition (Figure 6H). hA3G mutants harboring individual amino acid substitutions (R24G and Y125G) displayed equivalent or moderately less inhibitory activity with comparable dimerization (Figures S3A and S3B). In addition, 5G(24–28) and 4G(124–127) mutations both negatively affect the ability of hA3G to inhibit HIV-1 infection (Figure S4). Taken altogether, these results indicate that the N-terminal amino acid residues 24–28 (RPILS) contribute to the oligomerization of hA3G and its anti-*Alu* retrotransposition activity.